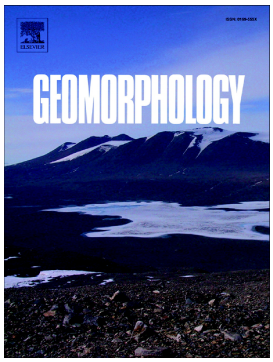

Three years of morphologic changes at a bowl blowout, Cape Cod, USA

Alex Smith, Paul A. Gares, Thad Wasklewicz, Patrick A. Hesp, Ian J. Walker

PII: S0169-555X(16)30331-2
DOI: doi: 10.1016/j.geomorph.2017.07.012
Reference: GEOMOR 6075

To appear in: *Geomorphology*

Received date: 19 May 2016
Revised date: 16 May 2017
Accepted date: 14 July 2017

Please cite this article as: Alex Smith, Paul A. Gares, Thad Wasklewicz, Patrick A. Hesp, Ian J. Walker , Three years of morphologic changes at a bowl blowout, Cape Cod, USA, *Geomorphology* (2017), doi: 10.1016/j.geomorph.2017.07.012

Three Years of Morphologic Changes at a Bowl Blowout, Cape Cod , USA

Alex Smith,
School of Environmental Sciences,
Univ. of Ulster, Coleraine
Co. Londonderry BT52 1SA No. Ireland
Smith-A22@email.ulster.ac.uk

Paul A. Gares,
Dept. of Geography, Environment and Planning
East Carolina University
Greenville NC 27837 USA
garesp@ecu.edu

Thad Wasklewicz,
Dept. of Geography, Environment and Planning
East Carolina University
Greenville NC 27837 USA
wasklewiczt@ecu.edu

Patrick A. Hesp,
School of the Environment, Faculty of Science & Engineering,
Flinders Univ.,
Bedford Park, So Australia 5042, Australia
patrick.hesp@flinders.edu.au

Ian J. Walker
School of Geographical Sciences and Urban Planning
Arizona State University
Tempe, AZ, 85287-8313
ianjwalker@asu.edu

Corresponding Author: Paul Gares, (garesp@ECU.EDU)

Abstract

This study presents measurements of blowout topography obtained with annual terrestrial laser surveys carried out over a three-year period at a single, large bowl blowout located in the Provincelands Dunes section of Cape Cod National Seashore, in Massachusetts. The study blowout was selected because its axis is aligned with northwest winds that dominate the region, and because it was seemingly interacting with a smaller saucer blowout that had recently formed on the southern rim of the primary feature. Assuming that blowouts enlarge both horizontally and vertically in response to the wind regime, the objectives of the study were to determine both the amount of horizontal growth that the blowout experiences annually and the spatial patterns of vertical change that occur within the blowout. Changes to the blowout lobe surrounding the feature were also determined for areas with sparse enough vegetation cover to allow laser returns from the sand surface. The results show that the blowout consistently expanded outward during the three years, with the greatest expansion occurring at its southeast corner, opposite the prevailing winds. The most significant occurrence was the removal, in the first year, of the ridge that separated the two blowouts, resulting in a major horizontal shift of the southern rim of the new combined blowout. This displacement then continued at a lesser rate in subsequent years. The rim also shifted horizontally along the northwest to northeast sections of the blowout. Significant vertical loss occurred along the main axis of the blowout with the greatest loss concentrated along the southeast rim. On the lobe, there were large areas of deposition immediately downwind of the high erosion zones inside the blowout. However, there were also small erosion areas on the lobe, extending downwind from eroding sections of the rim. This study shows that: 1. blowouts can experience significant areal and volumetric changes in short periods of time; 2. significant changes may occur relatively suddenly when adjacent blowouts combine into a single feature; and 3. the sediment transport paths are highly controlled by the topography. The joining of two blowouts not only creates a new larger feature, but it also releases large amounts of sediment that are then distributed across the landscape downwind, creating a potential for major changes to a landscape over the longer term.

KEYWORDS: Blowout, rim expansion, airflow, lobe deposition, wind events, terrestrial laser scanning

1. Introduction

Blowouts are common erosional features in coastal aeolian landscapes, often serving as sediment transfer corridors to inland locations (Carter et al., 1990; Gares and Nordstrom, 1995; Hesp, 2002; Anderson and Walker 2006). Blowouts develop in response to wave and aeolian processes, climate change, reduction or loss of vegetation cover, or anthropogenic disturbances (Carter et al., 1990; Hesp, 2002; Hesp and Walker, 2013). As blowouts evolve into saucer, bowl or trough shapes, the topography greatly modifies the boundary layer conditions affecting velocity and directionality of airflow (Hesp, 2002; Hugenholtz and Wolfe, 2009; Hesp and Walker, 2012; Smyth et al., 2013), which in turn influences the continued evolution of the landform (Hugenholtz and Wolfe, 2006; Abhar et al. 2015). Acceleration and steering of airflow has been the focus of a number of blowout studies (Hesp and Hyde, 1996; Hesp and Pringle, 2001; Hugenholtz and Wolfe, 2009; Hesp and Walker, 2012; Smyth et al., 2012, 2014; Pease and Gares, 2013, Gares and Pease, 2014), whereas other studies have examined long-term morphologic changes of blowouts (Gares and Nordstrom, 1987; Jungerius and van der Meulen, 1989; Carter et al., 1990; Gares and Nordstrom, 1995; Hugenholtz and Wolfe, 2006; Kayhko, 2007; Abhar et al. 2015). Studies that examine blowout topography over time have often focused more on changes within or along the margins of the blowout (Jungerius et al, 1981; Jungerius and van der Meulen, 1989; Pluis, 1992; Gares, 1992; Byrne, 1997; Hugenholtz and Wolfe, 2006) rather than on areas adjacent to the blowout. Although the blowout depression is essentially an erosional feature, its continued evolution has repercussions on the broader landscape, particularly in the growth of the adjacent depositional lobe that results from the excavation of sand within the blowout (Carter et al., 1990; Gares and Nordstrom, 1995; Brown and Arbogast, 1999; Hansen et al., 2009; Abhar et al., 2015).

This paper analyzes morphologic changes of a bowl blowout in the Cape Cod National Seashore, highlighting the dynamic nature of the blowout as it responds to fall and spring storms. Whereas previous studies of blowout topographic change often employed erosion pins or aerial photography as the source of data to monitor the evolution of blowout topography, this research relies on high-resolution topographic data collected by terrestrial laser scanning (TLS). Annual surveys carried out at the study site over a three-year period reveal patterns of sediment transport, blowout growth, and corresponding changes along the blowout margins and within the depositional lobes. The modifications to the blowout and adjacent features are attributed to the wind characteristics, particularly to individual storms that dominated during the

intervals between the surveys. The observations presented here provide detailed complementary information to the longer-term study by Abhar et al. (2015) about blowout evolution.

A secondary contribution of this research is the use of terrestrial laser scanning (TLS) to collect data, which offers significant improvement in the resolution and accuracy of topographic data over traditional survey methodologies used previously (e.g. Jungerius & van der Meulen, 1989; Pluis, 1991; Gares, 1992; Andrews et al., 2002; Hugenholtz and Wolfe, 2006; Kayhko, 2007; Hansen et al., 2009; Ollerhead et al., 2013). All of these approaches face interpolation issues in the production of accurate digital elevation models, particularly when attempting to represent the small-scale features found in many blowouts. Such methods may also result in the modification of the landform due to the pedestrian activity involved in data collection. Moreover, time constraints either limit the size of the survey areas or the frequencies of the surveys and a full understanding of how a landscape or landform evolves is hampered as a result. TLS is employed in this study to remove these shortcomings. This technology has been used increasingly and successfully in non-coastal systems (Bitelli et al., 2004; Milan et al., 2007; Wasklewicz and Hattanji, 2009; Hodge et al., 2009; Resop and Hession, 2010; Staley et al., 2011;), but its use is also increasing in studies of coastal environments (Pietro et al., 2008; Olsen et al., 2009; Nield et al., 2011; Dewez, et al., 2013; Feagin et al., 2014). Recently, TLS has been used to measure small bedforms and grain characteristics in aeolian and riverine systems (Nield and Wiggs, 2011; Brasington et al., 2012). Repeat TLS surveys provide accurate and precise measurements of blowout topography facilitating not only the identification of patterns of elevation change, but also the computation of volumetric sediment loss and gain in different locations across the landscape. In this way, this detailed study of landform change complements the broader aerial photographic examination of blowout evolution (Abhar et al., 2015).

2. Blowout Morphodynamics

Coastal blowouts tend to develop in moderate to high-energy wind environments and can generally be classified as having one of three primary forms: elongated troughs and circular saucer or bowl shapes (Carter et al., 1990; Hesp, 2002; 2011; Hesp and Walker, 2012). Blowouts have relatively distinct process-form relationships where their topographic characteristics are inextricably linked to flow steering, complex flow separation, and acceleration/deceleration of airflow with significant positive feedback between form and flow

(Hugenholtz and Wolfe, 2009; Hesp and Walker, 2012, 2013; Smyth et al., 2012, 2013, 2014; Pease and Gares, 2013; Gares and Pease, 2014). The primary axes of blowouts tend to be oriented in the direction of the dominant or prevailing regional winds competent for transporting sediment, but sometimes also the highest magnitude winds (Gares and Nordstrom, 1995; Hesp 2002; Hugenholtz and Wolfe, 2009). In trough blowouts, incoming winds aligned with the blowout axis are steered along the axis, but when wind approach angles are more oblique to perpendicular to the axis, significant topographic flow steering occurs (Hesp and Pringle, 2001), and recirculation zones develop in which air flows opposite to the incident wind direction (Hesp and Hyde 1996; Fraser et al., 1998; Hansen et al., 2009; Hesp and Walker, 2012; Pease and Gares, 2013). Airflow may decelerate as it enters the blowout in response to flow expansion, but usually becomes compressed as it moves up the axis and accelerates toward the crest of the blowout rim (Gares and Nordstrom, 1995; Hesp and Hyde, 1996; Hugenholtz and Wolfe, 2009; Hesp and Walker, 2012; Gares and Pease, 2014). As air exits the blowout over the crest and depositional lobe, airflow radially expands and localized flow separation zones may result in reduced wind speed and/or flow recirculation (Carter et al., 1990; Gares and Nordstrom, 1995; Hesp and Hyde, 1996; Fraser et al., 1998; Hesp, 1999, 2002; Smyth et al., 2012).

Blowouts can evolve from smaller notches and saucers in dune ridges into longer and deeper troughs and bowls through or on the ridge (Cooper, 1958; Gares and Nordstrom, 1995; Hesp and Walker, 2012), facilitated by incoming winds that are steered along the axis (Hesp and Pringle, 2001; Hansen et al., 2009) for troughs, or circulating within the saucer or bowl (Hugenholtz and Wolfe, 2009). Expansion of the blowout may decline or cease when a blowout becomes too wide to produce accelerated or competent flows that facilitate sediment transport and continued erosion (Carter et al., 1990; Gares and Nordstrom, 1995; Hesp, 2002). Blowout size and development can also be limited by erosion down to a surface (e.g. moist sand above or within the water table, a deflation lag, paleo-soils, calcrete layers etc.) that restricts further deflation (Gares, 1992; Hesp, 2002; Hugenholtz and Wolfe, 2006; Hesp and Walker, 2012, 2013). Gares and Nordstrom (1995) proposed a cyclical model of blowout evolution, which includes initiation, expansion, and eventual stabilization of blowouts after a critical size threshold has been reached. Others have observed gradual decay of blowouts over time (Carter et al., 1990), or a transition from large blowouts, especially trough blowouts, to parabolic dunes in which the critical size of the blowout was never fully reached because of

abundant sediment supply and high magnitude winds (Hugenholtz and Wolfe, 2006; Hansen et al., 2009).

A number of seasonal factors play a role in the initiation and development of blowout features. The most critical factor is the wind regime, which can involve significant seasonal variations at mid-latitude locations due to changes in frontal patterns. A number of other climatic factors, including precipitation, temperature, and evaporation rate, influence the effectiveness of aeolian processes to change the landscape (Davidson-Arnott and Law, 1990; McKenna-Neuman, 2004; Hugenholtz and Wolfe, 2006; Davidson-Arnott et al., 2007; Darke and McKenna-Neuman, 2008; McKenna-Neuman and Sanderson, 2008; Delgado-Fernandez and Davidson-Arnott, 2011). The climatic conditions, in turn, affect the vegetation cover that alters the wind's ability to transport sediment by modifying the vertical pattern of wind speed and stabilizing the dune surface (Olson, 1958; Bressolier and Thomas, 1977; Dong et al., 2001). The deflation potential is also influenced by surface conditions, including the size of the sand grains, the moisture content within the sediment matrix, snow cover, salt and biological crusts and the frozen condition of the surface (Davidson-Arnott and Law, 1990; McKenna-Neuman, 1993; McKenna-Neuman et al., 1996; Byrne, 1997; Langston and McKenna-Neuman, 2005; Hugenholtz and Wolfe, 2006; Davidson-Arnott et al., 2007). Many of these factors are enhanced in the winter, especially in latitudes above 40^0, when temperatures are low and days are short, conditions that inhibit evaporation, increase sediment moisture content, and promote frozen ground and accumulation of snow (McKenna-Neuman, 1993). All these conditions limit sediment transport in a season when wind speeds are frequently competent and vegetation cover is least dense, as at Cape Cod. During the summer, higher temperatures and long days produce significant evaporation that results in dry sand surfaces that would be susceptible to deflation, but wind speeds are generally lower and vegetation density greater than in winter. The significant difference in seasonal variations in solar radiation can be significant in affecting surface drying and sediment movement particularly on steep slopes (Oke, 1978; Hugenholtz and Wolfe, 2006). Overall, the winter conditions at Cape Cod would seem to have the greater potential for aeolian sediment transport because of the occurrence of storm events that involve extreme wind speeds, sufficient to overcome the factors that limit sediment movement, (Byrne, 1997; Delgado-Fernandez and Davidson-Arnott, 2011; Ollerhead et al., 2013; Hesp and Walker, 2012; Yurk et al., 2014; Abhar et al., 2015).

3. Study Site

The study site is located within the Provincelands Dunes, an 1800 ha undeveloped dune system within Cape Cod National Seashore at the northern end of Cape Cod (Fig. 1). The Provincelands Dunes include a Holocene parabolic dune complex located mainly in the eastern section of the dune field that contains several large, discrete parabolic dunes, which extend inland from the beach. The western section of the dune field consists of an aggrading spit with a wide foredune/relict foredune system of one to three dune ridges that parallel the beach (Forman et al., 2008). Blowouts are common features in this dune system, developing mainly on the seaward (north) sides of the dune ridges and of the trailing arms of the parabolics. Relying on remotely sensed imagery, Abhar et al. (2015) determine that Provincelands blowouts expand and contract differently during the time periods examined, seemingly in response to varying climatic and vegetation conditions.

The large dunefield attests both to the continued input of sediment transported northward along the beaches of Cape Cod (Forman et al., 2008) and to the wind regime that exists in this area. During the winter months, dominant winds blow from the north and west with a notable percentage of occurrences exceeding 11 ms^{-1} (see wind rose in Abhar et al., 2015). South and southwest winds dominate, occurring over 40% of the time, but wind speeds rarely exceed 11 ms^{-1}. During the fall and spring transitional periods, a bi-directional pattern develops with the majority of winds split between the north and south. Overall, the resultant vectors reflect the dominance of northwesterly winds, particularly in fall and winter, but in summer the resultant vector is from the southwest.

For this study, we focus on a large bowl blowout (42°04'46.35"N, 70°12'29.31"W), which developed on the seaward slope of an interior dune ridge (Fig. 2A), located roughly 340 m inland from the shoreline. The orientation of the long axis of this blowout (herein identified as blowout A) is approximately 292°, providing exposure to northwest and north winds (see also Fig. 3). The active surfaces of the blowout deflation basin and adjacent slopes are free of vegetation, while the depositional lobe and surrounding downwind slopes are covered with vegetation of varying density, mainly consisting of American Beach Grass *(Ammophila breviligulata).* Hairgrass *(Deschampsia flexuosa)* and beach heather *(Hudsonia tomentosa)* are also widespread on the more stable margins of the blowout. Several other floral species also grow on the depositional lobe, including poison ivy *(Toxicodendron radicans),* as well as woody shrubs and bushes such as Northern Bayberry *(Morella pensylvanica)*, and Beach Plum *(Prunis maritime).* The beach grass often loses vitality, dies back or becomes buried during the

winter months while the woody species become ‘islands’ that appear to be resistant to erosion year round.

During field reconnaissance of the site in April 2008, a small saucer blowout (referred to here as blowout B) was observed just landward of the blowout rim (Figs. 2A, 3). Aerial photography from May 2010 indicates a second small saucer had developed east of the first, separated by a small ridge (Fig. 2B). By May 2011, the two saucers had coalesced into a single small bowl blowout that had widened and lengthened considerably in a single year from 2010 to 2011 (Figs. 2C, 3).

4. Methodology

4.1 Data Collection and Uncertainty

Six TLS surveys were carried out at the study site (May 2011, May 2012, October 2012, May 2013, October 2013 and May 2014) using a Leica HDS C-10 tripod mounted scanner and following techniques documented in several previous studies (Staley et al., 2011, 2014; Scheinert et al., 2012; Wester et al., 2014; Wasklewicz and Scheinert, 2016). Leica HDS planar targets allow data collected at multiple scan positions in each of the field surveys to become seamlessly integrated into one point cloud through the registration process in Leica’s Cyclone software. Target positions were geo-referenced using an RTK GPS. The accuracy of integration of the data obtained from all scan positions is assessed by propagating the Root Mean Square Error (RMSE) and the Standard Deviational Error (σ) of the surveys throughout the scan series (Staley et al., 2011; 2014). Our analysis of the DEM uncertainty provides a global error measurement based on local control points at the study site. The propagated error budgets for the x, y, and z values are calculated to assess the level of uncertainty associated with the scan data and to assign error at the individual pixel level. Total (X,Y,Z) error is then used to give a ± value for the volumetric measurements based on the area of the zones where topographic changes occurred. For the surveys collected at the study site, the σ error values were slightly elevated overall and these measures provide a conservative level of uncertainty in the volumetric changes measurements (Table 1).

Table 1: Standard deviational error associated with individual TLS surveys and the propagated error between successive scan series. Note: for the analysis of the depositional lobes only annual scan series were considered (i.e. May to May) and the total (x,y,z) propagated error for years 2 and 3 are 3.58 mm and 10.36 mm, respectively.

Survey	$x_{(mm)}$	$y_{(mm)}$	$z_{(mm)}$	$Total^{(x,y,z)}_{(mm)}$
May-11	0.90	0.78	0.81	1.44
May-12	1.62	1.35	1.24	2.44
Oct-12	4.53	5.11	1.97	7.12
May-13	1.54	1.51	1.47	2.61
Oct-13	2.21	2.80	3.03	4.69
May-14	4.87	3.83	7.88	10.02
Propagated	$x_{(mm)}$	$y_{(mm)}$	$z_{(mm)}$	$Total^{(x,y,z)}_{(mm)}$
May11-May12	1.85	1.56	1.48	2.84
May12-Oct12	4.81	5.29	2.33	7.25
Oct12-May13	4.79	5.33	2.46	7.58
May13-Oct13	2.70	3.19	3.37	5.37
Oct13-May14	5.35	4.75	8.45	11.06

4.2 Vegetation Filtering and DEM Generation

Accurate geomorphic change detection (GCD) analysis requires the generation of bare-earth digital elevation models (DEM). This requires removal of data points that represent blades of grass and other vegetation that protruded above the surface outside of the blowout. Data cleaning is accomplished with LAStools software (Hug et al., 2004; www.rapidlasso.com) using a series of coded commands. First, a xyz point cloud from each TLS survey is imported into LAStools and converted to a .las file. The file is tiled into 10 m x 10 m point clouds with 1 m overlap. A two-phase filtering process is used because of the predominance of grasses and shrubs that are difficult to segment from the complex topography. Each tile is initially filtered using the extra-fine mode in LASground and a spike of 0.05, a step of 0.05, and offset of 0.01. After the LASground portion of the filtering the tiling process is reversed and the entire point cloud is thinned using LASthin. LASthin is performed for two specific reasons: (1) removal of any vegetation artifacts that would overestimate the bare earth surface; and (2) the production of a point cloud with consistent point spacing to remove the potential for spatial errors in the conversion of the points to a DEM. LASthin is process involved selecting the lowest elevation in a 10 cm area is selected during the LASthin portion of the filtering process. The filtered point cloud is then exported as a .tif file and converted in ArcMap v.10.x to a raster grid. A 10 cm planimetric raster size is selected to reduce the influence of residual artifacts from vegetation, as previously mentioned and reduce any vegetation shadows while still maintaining a high level of spatial resolution. Micro relief features such as grain avalanches, ripples and footprints are still visible. From here the DEM is transformed into various raster surfaces to further study blowout morphometry (e.g. slope mapping, curvature, hill shade etc.).

4.3 Geomorphic Change Detection

The evolution of the blowout is analyzed using the gross areal and volumetric changes between successive pairs of scan surveys. For this study, we focus on changes on the inner erosional basin of the blowout and the outer depositional lobe. The inner basin is established by identifying the location of the blowout rim, which is determined by examining the slopes up the sidewalls of the blowout and down the gentler lobe slope. The rim corresponds to the highest peak that separates the two sloping surfaces. The slope aspect and curvature functions available in ArcMap are also used to help identify the rim position, as these parameters visibly changed from one side of the rim to the other (e.g. west-facing vs. east-facing slopes). It was difficult to precisely identify the crest location at some locations including the northwestern entrance to the blowout where there was neither an obvious ridge crest nor an obvious change in slope aspect. Rim identification was also difficult at the southeastern corner of the blowout, where, in the more recent surveys, considerable erosion occurred lowering the rim to create a gently sloping corridor to the lobe. These areas required careful examination of the slope and aspect data to establish the rim and ultimately rim identification involved considerable subjectivity.

With the blowout rim established, polygons representing the inner, erosional blowout zone were created in ArcMap, allowing for the calculation of areal dimensions for each survey. The evolution of the blowout area could be compared through time. In addition, the identification of the blowout rim allows a determination of the amount of horizontal displacement that occurred around the blowout. Displacement was quantified by establishing 16 transects in angular increments of 22.5^{o} across the study area from an arbitrarily defined center point of the blowout (Fig. 3). Using the ArcGIS measuring tool, the horizontal distance along each transect from the center point to the intersection with each successive blowout rim line is determined. Comparing pairs of distance values along each transect establishes rim displacement during one-year time intervals.

Volumetric changes through time were computed for both the inner blowout and outer lobe zones by comparing elevation values for each cell in sequential DEM's. Cell volume change was determined by using the elevation change value and the cell area (10 cm^2); volume changes for the cells within the polygon of interest are summed to establish the total volumetric change. Accepted error for the volumetric estimates is based on the sigma value of 8.5 mm in the vertical, as described above. The cell volumetric change data are also mapped

in ArcGIS to depict the patterns of erosion and deposition across the two zones of interest (Staley et al., 2011, 2014; Scheinert et al., 2012; Wester et al., 2014; Wasklewicz and Scheinert, 2016).

Whereas deriving areal and volumetric data for the blowout was facilitated by the relative ease of establishing its boundary, determining the outer lobe boundary proved more difficult due to the subtle nature of the terrain outside of the blowout itself. Initially, we focused on the two blowouts and a limited area beyond the blowout rim, which we assumed would be the zone of deposition. As we became aware that deposition extended well beyond the original survey area (see also Abhar et al., 2015), we realized the importance of maximizing coverage in this zone and we expanded the scanned area in subsequent surveys. A secondary issue with scanning outside of the blowout was the vegetation across the lobe. A large proportion of the area was covered by dune grasses with low to moderate densities, and data points that reflect the grasses can easily be clipped from the point cloud. In some areas, however, vegetation cover was quite dense, and, despite our best efforts to scan from numerous points to maximize bare earth hits, the point densities were low for these locations. Therefore, there are areas within the lobe zone for which there are no data. These zones tend to be located at the outer extremities of the lobe zone where their presence hampers the ability to define a consistent boundary for the lobe. In order to provide some limit for the analyses, we decided to arbitrarily draw boundaries on the maps that maximized the amount of volumetric change data available, while minimizing the area of limited data coverage. As a result, the boundaries of the first pair of surveys produce a smaller lobe zone than those of the latter surveys which had an increased number of scans that expanded the coverage area and penetration in areas of denser vegetation. Determining areal dimensions for the lobe zone is of little value because of the changing boundaries, but volumetric changes are quantified. It should be noted that the volumes reported represent total volume for a changing polygon area. To normalize these volumetric data and facilitate comparison between time intervals, changes are reported as volumes per unit area (m^3m^{-2}), in addition to the total volume change.

4.4 Wind Regime

Wind conditions during the study period (May 2011 to May 2014) were determined using data collected at one hour intervals at the Provincetown airport (located 0.75 km west of the study blowout), the same station used by Abhar et al. (2015) to characterize the long-term wind regime. Because the TLS topographic surveys were carried out in May and October, we

divide the wind year into a summer season (May 1 through October 31) and winter (November 1 through April 30 the following year). Wind conditions during the study period were consistent with the long-term trends (see Fig. 1 in Abhar et al., 2015). Conditions during the full study period closely resemble the long-term conditions reported by Abhar et al. (2015).

Identifying wind conditions favorable for sediment transport involves first establishing a threshold of motion wind speed for sediment conditions at a particular location (Fryberger and Dean, 1979). Delgado-Fernandez and Davidson-Arnott (2011) focus on shorter individual events in an attempt to equate them to sediment transport conditions during the event or to topographic changes that occur as a result of the event. They too use a threshold of motion wind speed for data collected more frequently at the site, and they focus on events with a minimum of 2-hour durations. In this study, we are interested in topographic changes in a full circle around the blowout and, therefore, we separate events not only according to their wind speeds but also their directional component. In this study, we use a 3-hour minimum duration for defining events, which emphasizes slightly the longer events. The threshold of motion is determined from local sediment conditions characterized by 16 sediment samples collected in October 2012 at randomly selected locations in the blowout. Using mean grain size and sorting values (Folk, 1966), we established that 95% of sediment particles at this site would be expected to be larger than 0.681 mm. This conservative estimate of sediment size was used to determine a minimum event wind speed following Bagnold's (1941) threshold shear velocity equation and the law of the wall equation. The surface threshold shear velocity converts to wind speed of 9.47 ms^{-1} at the 10 m height at which standard meteorological wind data are recorded.

The event segregating conditions are then applied to the hourly wind data collected at the Provincetown meteorological station, starting with the removal of all values below the threshold speed, and then eliminating situations with less than three consecutive hours of wind speeds above the threshold. Finally, the event must have a relatively consistent direction, with data values all within a 60^{o} range. We then calculate an average wind speed and wind direction for the event and record the event's duration.

Applied to all the Provincetown data, this procedure results in the identification of 98 wind events for 2011-2014. The seasonal distribution of events shows that there are significantly more wind events in the winter than in the summer (Fig. 4) and over 50% of those involved winds come out of the northwest. However, northeast wind events had the highest

wind speeds and longest durations with three of the 12 northeast events lasting more than 2 days, and 5 of the events having average speeds above 12 ms^{-1}.

4.5 Sediment Drift Analysis

The influence of the blowout topography on sediment redistribution within the blowout is determined for each study year by comparing the expected patterns of sediment transport for the study period, as determined by Fryberger and Dean's (1979) Drift Potential (DP) values, to the observed changes derived from the TLS topographic change data. Following the Fryberger and Dean procedure and the recommendations of Bullard (1997), the sediment transport threshold velocity (9.47 ms^{-1}) establishes the lower limit of wind speed classes, with each class representing a 2 ms^{-1} range. In addition, to reduce computation error (Pearce and Walker, 2005), we use the mean of the recorded occurrences for each class and we ensure segregation between classes by cutting off each class at 0.9 ms^{-1}.

To calculate the observed volumetric changes in a way that makes them comparable to the DP values, we established 16 directional transects from the blowout basin center to the blowout rim and determined total volumetric change for a two pixel-wide band along each transect. Because the predicted and observed data are reported in different units, the drift potential (DP) and volumetric loss for each directional transect are then converted to a percentage of the total for all 16 transects.

Fryberger and Dean (1979) proposed an integration of individual DP values for each directional class into a single resultant vector, the resultant drift direction (RDD). Here, we apply the Fryberger and Dean procedure to the observed measurements of net volumetric change within the blowout along the directional transects to create an observed resultant drift direction that can be compared to the predicted RDD to determine how the local topography influences the actual sediment transport pattern.

5. Results

5.1 Blowout Morphometric Changes

The initial survey in May 2011 shows the positioning of the large bowl blowout (A) and the saucer blowout (B) located just south of the bowl blowout rim (Fig. 3). Over the three years of observation, blowout A expanded outwards, capturing blowout B in the first year. The mean

of the 16 measures of rim displacement along the sampling transects (Fig. 5A) was greatest during winter periods (0.5 to 0.9 m on average for the entire blowout rim), but almost negligible during the summer periods. As a result, the focus of the analysis is on the annual changes, which reflects blowout adjustment that took place primarily during the winter. Fig. 6B is a radial plot of the cumulative changes along each transect. The breach that occurred between blowouts A and B is not depicted on the figure; rather the data represented for the south-southeastern transects show the displacement of the outer rim of blowout B which became the outer rim of blowout A once the two merged. The radial plot (Fig. 5B) shows that the south rim of blowout B shifted outward by up to 2.5 m during the first year at the same time that the ridge between the two blowouts was removed. This rim section continued to expand not only to the south but also increasingly in southeasterly direction in 2012-2013 and more so in 2013-2014. Two other zones of moderately large rim retreat were along the northwestern and eastern sections of the blowout where total horizontal expansion reached 4 m over the 3-year study period. The northeast and southwest sections of the rim retreated only by 1 to 2 m during the total interval.

The rim displacement resulted in changes to the blowout area. The first survey revealed that blowout A covered 1948.6 m^2. During the first year, the total blowout area increased by 563.3m^2 or 28.9% of its original area (Table 2). The majority of this growth (85%) was due to the incorporation of blowout B as part of the larger blowout. During the subsequent years, the blowout continued to increase in area, adding 858m^2 to the overall area by May 2014. Overall, the blowout grew by 30.6% of its original area, with about two thirds of that growth associated with the capture of blowout B.

As the blowout was expanding outward, it also had vertical changes that resulted in a net loss of 2487.2 m^3 of sediment over the three-year study period (Table 2). The central axis of blowout A was the predominant erosional area, with the greatest amount of sediment loss located at the south-southeastern end (Fig. 6). In 2011-2012, over 1.5 m of vertical loss occurred at the ridge separating blowout A from blowout B, and erosion in this area continued over the next two years, resulting in 3.75 m of total vertical loss (Fig. 8A). Between 2012 and 2014, this erosion zone shifted slightly to the east where the surface eroded downwards 1.5 – 2m (Figs. 6, 8C, 8D). Sediment removal also occurred in the center of blowout A where up the elevation was lowered by up to 2 m (Fig. 8B).

Table 2: Areal (m^2) and volumetric changes (m^3) in the blowout erosional basin and on the depositional lobe. Category "Area No Data" refers to the size of the area within the zone defined as the lobe on each map for which there was no elevation data due to vegetation density.

Time Interval	Area Change m^2	Erosion m^3	Deposition m^3	Net Change m^3	
Erosional Basin					
May11-May12	563.3	855.4 ± 5.7	221 ± 1.4	-634.4 ± 7.1	
May12-Oct12	9.2	7.9 ± 1.9	37.1 ± 16.8	29.2 ± 18.8	
Oct12-May13	106.4	873.2 ± 17.6	14.7 ± 2.3	-873.2 ± 19.9	
May13-Oct13	-0.76	14.0 ± 4.7	25.6 ± 9.4	11.6 ± 14.1	
Oct13-May14	179.8	1028.4 ± 28.6	8.2 ± 2.4	-1020.4 ± 31.1	
Total:	858	2750.9 ± 58.5	306.5 ± 32.3	-2487.2 ± 91.0	
	Total Area m^2	**Erosion m^3**	**Deposition m^3**	**Net Change m^3**	**Area No Data m^2 / %**
Depositional Lobe					
May11-May12	4101.9	310.1 ± 4.8	170.1 ± 4.1	-140.0 ± 8.9	925.4 (22.6)
May12-May13	9901.4	93.9 ± 4.1	1045.6 ± 23.3	951.7 ± 27.4	1005.0 (10.1)
May13-May14	9901.4	509.4 ± 29.1	700.8 ± 50.5	191.4 ± 79.6	801.7 (8.1)
Total:		913.4 ± 38.0	1916.5 ± 77.9	1003.2 ± 115.9	

There were few areas of deposition within the blowouts, and in those areas elevation gain was for the most part under 1 m (Fig. 7). The exception to this occurred in 2011-12 when 1.5 m of sediment accumulated on the floor of blowout B (Fig. 7 transect 1). This deposition was almost certainly the result of the erosion that occurred along the ridge separating blowouts A and B, which would have released a large quantity of sediment to be blown into the bottom of blowout B by the northwest winds that flowed through blowout A. This deposited sediment was removed in subsequent years, presumably moved over the rim to the depositional lobe to the south and southeast. Other areas of minor deposition (< 0.6 m) are located on the northwestern and northeastern sidewalls (Fig. 7 transect 2), and in the lowest part of the blowout floor. These deposition zones appear to be somewhat ephemeral, appearing in some years and disappearing in others. Indeed, whereas the data show the gain of 306 m^3 of sediment over the study period (Table 2), 221 m^3 represented the deposition of sand in the bottom of blowout B during the first year and these sediments were removed from that location in subsequent years (Fig. 7 transect 1). Thus, gross volumetric gain to the blowout amounted to only about 80 m^3 over the 3-year period.

While the central section of the blowouts, especially at the southern end, were highly erosive during the study period, the lateral walls were areas of much more subtle changes. The west-southwest section of the wall of blowout A remained nearly unchanged throughout the study period (Fig. 7 transect 2). However, the northern wall was more active, and included a zone of both vertical (<1 m) and horizontal (<5 m) erosion at the base, a stable area in the middle of the slope, and an erosional zone in the upper section of the wall (Fig. 7 transect 2). Parallel horizontal slope retreat (~5 m in both cases) is notable at both the wall base and crest. The upper rim section shows a simultaneous accumulation of sediment just over the rim onto the lobe. The parallel horizontal retreat of the sidewall along the northern side of the blowout is especially evident on the eastern section of the wall (Fig. 7 transect 3) where the entire slope was displaced horizontally by about 5 m.

Although the capture of blowout B by blowout A is the most obvious component of the evolution of these landforms, changes in southeastern corner of the new combined blowout reflect the topographic response to airflow through the blowout. The majority of the vertical changes in the blowouts during the 2012–2014 period occurred along the eastern and southeastern lateral walls of the blowout (Fig. 6). As noted, these sections of the wall showed parallel horizontal retreat of about 5 m during this period (Fig. 7 transects 3 and 4). At the same time, the rim at these locations was both displaced laterally and eroded downward. These changes at the blowout rim produced modifications to the topography some distance away from the rim (Fig. 7 transect 5). Accumulation of sediment on the lobe is evident at both the northern and southern ends of transect 5, reflecting the transfer of sediment from within the blowout to the outer lobe area. At the same time, the central part of the transect shows the existence of a deepening but also narrowing sediment transport corridor. Transect 4 (Fig. 7), that runs through the middle of this corridor, shows that the deepening was concentrated at the blowout end of the transect, and that a small amount of sand accumulated at the downwind end.

5.2 Depositional Lobe Elevation Change

Monitoring change on the depositional lobe is limited by the quality and density of elevation data collected. In 2011, the lobe area surveyed was limited in extent because the focus was initially on the changes inside the blowout. The initial TLS survey of the lobe was designed to give only a basic representation of the feature and there are large sections where

data is unavailable due to the density of vegetation cover and/or lack of survey coverage. In the following years, coverage of the lobe was expanded and more scans were carried out to fill in those areas with heavy vegetation cover, allowing for wider coverage of the lobe (Fig. 8) and a more accurate calculation of the volumetric changes. Despite improved survey density, vegetation cover still prevented accurate determination of elevation values in some places and these resulted in cells that lack data. The total area of the no data zones represented a decreasing percentage of the lobe area during the more recent time intervals (Table 2).

Over the three-year study period elevation changes on the lobe were variable in location and in size. Initially, there were large areas of erosion that extended from the rim of blowouts A and B, creating visible swales to the east of the rim (Fig. 8; see also Fig. 7 transects 4 and 5). The swales continued to erode at a lesser rate during the second and third years of study. Overall erosion in these areas amounted to as much as 1 m. At the same time, there was deposition in areas adjacent to these swales in all three years, resulting in the accumulation of about 0.5 m. The 2012-13 and 2013-14 maps show an extensive deposition zone to the southeast of blowout B, with nearly a meter of sand accumulated in certain locations over the three-year period. Other lesser deposition zones (up to 0.5 m) existed to the east of the rim of blowout A. The lobe area to the south of blowout B was another erosional area in 2011-12 and 2013-14, with erosion reaching 0.5 m in some places.

Total volumetric changes computed for the lobe zone, based on the available data, indicate that there was continual accumulation of sediment during the 2011-2014 period (Table 2). The volumetric data for 2011-12 suggest that erosion prevailed across the lobe, but the area covered by the survey did not extend very far beyond the rim so that areas of likely deposition further downwind are not accounted for. The 2012-13 and 2013-14 maps, representing a larger scanned area, show that the deposition zones did extend well beyond the lobe boundary used in 2011-12. Thus, the volumetric data show that during the last two years of study, the lobe had a net growth of just over 1000 m^3 of sand, which amounts to 0.1 m^3m^{-2}.

5.3 Wind Events and Sediment Drift Potential

Fig. 10 presents the distribution of wind events for each year of study, along with the DP values and the erosion data for the sample transects. Originally, Fryberger and Dean (1979) presented the DP's expressed as vector units in rose form corresponding to the

directions from which the wind blew. Here, they are presented according to the direction in which the wind blows so that they can be compared to the erosion data.

For the period 2011-2014, we identified 98 high magnitude events, 88% of which occurred in the winter months, (November – April). There were slightly more events in 2011-12 (38) than in 2012-13 (32) or 2013-14 (28) (Fig. 9). Overall, 56.1% of events had northwest wind directions, with another 27.5% from the southwest. However, the annual distribution of wind directions was different in each year. Events with directions from the northwest occurred most frequently in 2012-13 and 2013-14; southwest events occurred more frequently in 2011-12 (Table 3). There were also differences in average wind speeds associated with each direction in each of the study years. In terms of duration, 53% of events lasted 12 hours or less, and 14% lasted 24 hours or more.

Table 3: Frequency distribution and average speed of wind events by quadrant for each study year; highest values for each year shown in bold

	2011-12		2012-13		2013-14	
Quadrant	**Freq. (%)**	**Mean Speed (ms^{-1})**	**Freq. (%)**	**Mean Speed (ms^{-1})**	**Freq. (%)**	**Mean Speed (ms^{-1})**
NE	13.2	10.72	23.3	**12.37**	10.7	11.70
SE	5.2	11.04	13.3	11.90	7.1	**11.89**
SW	**47.4**	**11.16**	10.1	12.05	38.6	11.31
NW	34.2	11.09	**53.3**	11.19	**53.6**	11.38

Of the 98 high-speed events, 16 had average speeds of 12 ms^{-1} or greater. These events often had several consecutive hours of wind speeds in the 15-17 ms^{-1} range, with maximum speeds of 20 ms^{-1}. Wind directions associated with these highest magnitude events were fairly evenly distributed, although there were slightly more events from the southwest and northwest. These events also tended to have long durations, averaging 26.9 hours. There were 2-3 such high magnitude/long duration events in each of the study years mainly with west or northeast directions, although one event in 2011-12 did have south winds. 2012-13 was particularly notable, with 3 events whose average speeds were 14-14.5 ms^{-1}, and average duration of 36 hours.

The DP distribution is greatly affected by high magnitude/long duration events associated with particular directions (Fig. 9). This is seen in all three study years. In particular, in 2012-13 two significant northeast storms account for over 35% of the total annual drift, and a

strong northwest event is responsible for another 15%. Thus, these three significant events produce 50% of the total sediment drift potential for 2012-13. Similar situations can be identified in 2011-12 and 2013-14. Shorter duration events with high wind speeds are also associated with high DP's, and in 2011-12 when two high magnitude southwest events that lasted less than 24 hours account for 20% of the annual drift potential. Two moderate magnitude/duration northeast events in 2013-14 are responsible for 23% of the annual DP.

Comparing actual volumetric changes along transects to the drift potential shows significant differences between the two. In all years, actual erosion is greatest along the northwest-southeast axis and least along the northeast-southwest axis. In each of the three years, about 50% of the total erosion occurred along transects located in the southeast quadrant. The only other notable erosion takes place along the northwest transect, varying between 8% and 15% of the total erosion from year to year. The greatest DP varies in each of the three years, but it conforms to the primary sediment transport direction only once, in 2013-13 along the 135^{o} transect. In that same year, the highest DP (32%) is along the 112.5^{o} transect whereas the actual erosion along that transect represented only 12% of the annual total. There is little to no potential drift to the northwest because there were few southeast wind events (Figure 9), but erosion was recorded along the 315^{o} transect.

The resultant sediment transport vectors, calculated following the Fryberger and Dean (1979) procedure to determine RDD, are quite consistent from year to year with an average direction of 146^{o} (Fig. 9). The resultant DP vectors are much more variable as the wind pattern distributions, and especially the occurrence of high magnitude events, differ from year to year. The consistency of the sediment transport patterns under highly varying wind conditions attests to the significant role that the topography plays in determining where erosion predominates.

6. Discussion

Our findings provide new insights into the spatial and temporal variations of a blowout erosional basin and associated depositional lobe. Previous studies that used aerial photographs to map changes to the overall shape of blowouts were unable to quantify accurately the amount of areal or volumetric change (Jungerius and Van der Meulen, 1989; Gares and Nordstrom, 1987; Gares and Nordstrom, 1995; Abhar et al., 2015). Studies that have been more successful at quantifying changes have often relied on sampling along

transects or surveying across a coarsely gridded area and, thus, suffer from poor spatial resolution (Pluis, 1991; Gares, 1992; Gares and Nordstrom, 1995; Andrews et al., 2002; Hugenholtz and Wolfe, 2006; Kayhko, 2007; Hansen et al. 2009). High-resolution laser scanning allows for highly detailed topographic mapping, which in turn facilitates using elevation differencing techniques that quantify the rapid changes to the morphologic units of the blowout. Information thus derived about landform change can be used to conceptualize the airflow characteristics that likely led to the landform response. It should be noted, however, that areas with denser vegetation cover hamper the ability of the scanner to yield data at a resolution comparable to other less-vegetated locations. It would be advisable to identify those areas in advance and then augment the TLS data with DGPS sampling. Integrating elevation data from sources with different resolutions is a difficult proposition (Wasklewicz et al., in review).

Initial visual inspection of blowout A suggested that, like most bowl-shaped blowouts, it was evolving through an interaction between the internal deflation basin and the depositional lobe located adjacent to the blowout beyond the rim. The blowout's basic orientation and the location of the main depositional area to the southeast point to the importance of northwesterly winds in the evolution of the landform. An interesting component of the feature was the presence of a small saucer blowout (B) on the southern rim of the blowout, which led to questions about the interaction between the two features. The first pair of surveys identified sudden large-scale blowout growth as blowout A expanded into and captured the smaller saucer blowout (B), which had been deepening and expanding independently before the merger. While previous research has alluded to the coalescence of blowouts (Gares, 1992; Gares and Nordstrom, 1995; Hesp, 2002), studies in Provincelands dunes have provided details about this type of landform piracy. Abhar et al. (2015) found that the merger of smaller blowouts with larger features (called "union events") was common over the longer term, occurring in 28% of the blowouts studied. Often the union of these blowouts is followed by a rapid phase of blowout development. The Abhar study demonstrates that this development phase occurs during a period of just a few years following the capture, and provides both accurate areal and volumetric quantification of the attendant changes. Initially, erosion of the ridge separating the two features resulted in removal of up to 2.5 m of sediment (Figs. 3, 6, 7), creating an opening that effectively joined the two landforms. During the same time frame, up to 1.5 m of sediment was deposited in blowout B, an accumulation that represented about 25% of the sediment eroded from the rim of blowout A. Although blowout capture increased the

overall size by more than 25%, the accumulation of sediment on the floor of blowout B diminished the net volumetric loss from the combined system (Table 2).

The expansion of the blowout towards the southeast is the result of the high frequency of high speed winds from the northwest (Fig. 9) that are most competent at transporting the rather coarse sediment that dominates the site. Previous work has shown that winds aligned along a blowout's axis tend to accelerate due to constriction created by the blowout and are realigned by the sidewalls of the blowout (Hesp and Hyde, 1996; Hesp and Pringle, 2001; Hesp and Walker, 2012; Smyth et al., 2012; Pease and Gares, 2013; Gares and Pease, 2015). In this blowout, the significant erosion that occurred along the ridge between blowouts A and B (Figs. 6, 7) likely was the result of the west to northwest winds during that first year (Fig. 9) that would have been redirected towards the south by the steeply sloped and high blowout erosional wall along the east side of blowout A. This redirection focused the wind on the ridge separating the two blowouts, resulting in ridge breaching.

The capture of blowout B has affected the evolving landscape in just the three years that followed the breaching of the ridge. The high blowout rim in the southeastern corner eroded laterally and vertically in the second and third years (Fig. transects 3 and 4), increasing the ability of the northwest winds to move sediment in that direction. The scouring of a trough through the crest in the southeastern corner of the blowout (Fig. transect 5) created a transport corridor that has facilitated the conveyance of sediment further inland, expanding the depositional lobe in an east-southeast direction (Fig. 8). Simultaneously, the displacement and lowering of the rim along the southern section of the blowout has facilitated movement of sediment in a more southerly direction, leading to the growth of the lobe in that direction (Fig. 8). Although blowout expansion through scouring of the floor and accumulation of eroded material on the lobe at the downwind end of the blowout has been noted previously (Jungerius and van der Meulen, 1989; Carter et al., 1990; Gares, 1992; Fraser et al., 1998; Hesp and Walker, 2012), the way the erosion of the blowout wall and rim modifies and then controls the airflow paths and sediment transport from inside the blowout to different parts of the depositional lobe has only been alluded to (Gares, 1992; Gares and Nordstrom, 1995). The continued evolution of this blowout will involve a feedback between the modified topography and the airflow that will produce additional topographic changes involving building up of certain parts of the lobe and continued erosion of sections of the southeast rim (Fig. 8).

Although the capture of blowout B was the most significant change, the main blowout also expanded through wall and rim displacement along the northeastern and northwestern margins, while the southwest section remained nearly stable (Figs. 3, 5). The nature of the rim changes does not reflect the distribution of wind events during the study period, as shown by the comparison of the drift potential patterns with the distribution of actual volumetric changes around the blowout (Fig. 9). Rim displacement along the northwest ridge was unexpectedly large given that southeast wind events occurred least frequently of all and with the lowest mean wind speeds. Notable migration was also recorded along the northeast rim of blowout A (Fig. 5, Fig. 7 transect 2) despite the fact that only two southwest wind events had average speeds in excess of 12 ms^{-1}. In contrast, there were few northeast wind events but the average speeds during these events were the highest recorded. Despite these favorable wind conditions, the southwest segment of the blowout rim underwent very little change during the study (Fig. 5, Fig 7 transect 2).

Given that correlation between changes to the northeast, northwest and southwest sections of the blowout rim and the wind distribution characteristics are poor, it seems likely that the measured rim changes are related to secondary flow characteristics such as those that develop on the lee slopes of transverse dune ridges. The width of the flow separation zone and the nature of the flow within that zone have been widely examined (Sweet and Kocurek, 1990; Walker, 1999; Bullard et al., 2000; Walker and Nickling, 2002, 2003; Parsons et al., 2004; Schatz and Herrmann, 2006; Walker and Shugar, 2013). One component of this flow that seems relevant to the blowout situation here is the width of the separation zone, which the research has been shown to be 3-15 times the dune height. The width of the separation zone is also dependent on the speed of the upwind airflow, with higher speeds resulting in reattachment further downwind. In the separation zone, flow becomes circular as the air falls to the surface and then flows back up the lee slope in the opposite direction to the flow at the crest. Flow may follow along the lee slope of a transverse dune in a helicoidal shape moving laterally along the slip face of the dune ridge when winds approach the ridge at an oblique angle. The direction of airflow along the lee slope is dictated by the angle of approach of the wind and would be expected to move in the same general direction as the wind, albeit locally redirected along the strike of the lee slope.

Applied to the study blowout, these principles suggest a hypothetical flow pattern (Fig. 10) that may prevail during storms with wind approach angles normal to the northeast and

southwest rims of the blowout. Based on the research concerning the distance to the reattachment point, and on the fact that the northeast dune rim is 8 to 12 m above the blowout floor, it can be assumed that flow reattachment would occur between 25 and 160 m downwind. During northeast storms, it seems logical that flow reattachment could occur beyond the opposite (southwest) blowout rim because of the height differential between the two ridges and because of the high velocities associated with the storm winds such as the northeast wind event in the fall of 2013 (Fig. 10A). The lack of rim displacement along the southwest ridge (Fig. 7 transect 2) suggests insufficient wind energy to produce change in that location, which supports this hypothesis. If this flow pattern applies to this situation, the blowout floor would be entirely within the separation cell, and flow reversal would occur up the blowout sidewall in the lee of the northeast rim. If wind direction shifts slightly north of northeast, a helicoidal flow would potentially develop moving along the sidewall to the southeast, toward the opening between blowouts A and B.

When winds blow from the southwest, a different flow pattern can be hypothesized (Fig. 10B) because the southwest rim crest only ranges from 3 to 7 m in height above the blowout floor and wind speeds during southwest wind events are lower than during northeast events. These conditions would be expected to create a reattachment point 10 to 100 m downwind, which in most cases would be within the blowout. The northeast ridge shows evidence of progressive lateral displacement during the study (Fig. 5), which could occur if the flow reattachment point was located on the upper northeastern sidewall. Southwest wind events did represent 27% of all events identified during 2011-14, and, although only two events had average speeds greater than 12 ms^{-1}, the winds speeds were sufficient to initiate sediment transport. The erosion of the northeast rim may well be associated with the occurrence of these events. The actual angle of approach of these events would also dictate the direction of sediment transport under these conditions. Winds from a more westerly direction would approach the northeast sidewall at an oblique angle that would cause a deflection in a southeast direction. For example, in 2013-14, the considerable sediment erosion in the southeast quadrant was facilitated by significant wind events from the west-southwest and west-northwest (Fig. 9). If the angle of approach were more southerly, the deflection of the wind would be toward the northwest along the northern sidewall. In 2011-12, there was considerable erosion in the northwest quadrant, when a large number of southwest events occurred, three with average wind speeds above 12.5 ms^{-1}.

Although local airflow data are missing here, the survey data do point to the influence of topography on steering the flow through the blowout, unlike the open beach where the difference between potential and observed transport is limited by moisture and fetch distance (Davidson-Arnott et al., 2007; Darke and McKenna-Neuman, 2008; Delgado-Fernandez and Davidson-Arnott, 2011). The large changes in elevation and shape at the southern end of the blowout attest to the funneling of air through the center of the blowout, as numerous others have noted (Hesp and Hyde, 1996; Fraser et al., 1998; Hesp and Pringle, 2001; Hesp and Walker, 2012; Smyth et al., 2012; Pease and Gares, 2013; Gares and Pease, 2015). The gradual shift of the primary area of change towards the east is facilitated by the development of a low trough through the former rim in that southeast corner which expanded both in width and depth through the three years of study. This area subsequently became an avenue for sediment to be moved to the lobe, as evidenced by the accumulation of sediment along its margins (Fig. 8). The occurrence of significant sediment loss on the north-northwest wall of the blowout in a location where southeast winds of any consequence rarely occur must be attributed to redirection of airflow that is approaching at an oblique angle to that wall, and in this case points to the significance of southwest winds that do occur over 25% of the time.

The laser scan data also provide information about the evolution of the depositional lobe. In this paper, we have defined this lobe as a broad feature that extends around about half the blowout. Its width was established by the availability of high quality scanned data, whereas the northeast and southwest boundaries were arbitrarily defined. The decision to define the lobe so broadly was motivated by the desire to determine the nature and magnitude of changes in areas that appear visually to be stagnant. However, changes in these particular areas amounted to as much as 20-30 cm per year, indicating greater aeolian effects than might be expected. However, deposition does not occur uniformly and consistently across the lobe. There are also distinct areas where significant erosion of the lobe (over 40 cm) occurred adjacent to areas with similar amounts of deposition within the same year (Fig. 8). Large erosional zones developed on the lobe at a time when capture of blowout B was taking place during the first year. The development of the erosional zone east of the northeast corner of blowout B (Fig. 6) would seem to be a direct consequence of the opening of the ridge between the two blowouts. Erosion in this zone continued during the entire study period, albeit at a decreased rate. A second area to the north also had significant erosion in 2011-12, but the amount of erosion and extent of the erosional area diminished in succeeding years. Unlike other studies (e.g. Hanson et al., 2009) that identify deposition on the lobe along the main axis

of the dune blowout with decreasing levels of deposition occurring in the periphery areas, this study shows deposition is far more widespread. A further insight resulting from this work is that the lobe can also be erosional in places, as might be expected in a relatively multi-directional wind regime.

The interconnectivity between the blowout and its depositional lobe and the availability of high quality elevation data begs the determination of a sediment budget for the combined features. However, for the three years of study, our data show a discrepancy of some 1400 m^3 of sediment between that which was eroded from inside the blowout and that deposited on the lobe (Table 2). The difference may in part be attributed to missing data associated with dense vegetation where low point densities prevented accurate determination of the bare earth surface. The lack of data in these places is unfortunate because the vegetation facilitates and stabilizes sediment deposition. Consequently, our measures of sediment accumulation in the depositional lobe are likely lower than actual deposition. In addition to the vegetation problem, the sediment budget for the lobe is limited by the size of the area scanned. The fewer scans completed in the first year resulted in limited data coverage of the lobe, but in subsequent years the added scans allowed us to expand data capture to larger portions of the lobe. Still, the discrepancy between erosion inside the blowout and deposition on the lobe would seem to imply that the unaccounted sediment must be transported beyond the lobe boundaries used here. The amount of retreat along the northern sections of the blowout rim might suggest that the eroded material is transported out of the blowout onto the adjacent lobe area, which was not included in our volumetric computations. This material no doubt accounts for some of the missing sand. It also seems highly likely that a considerable amount of sand was transported beyond the boundary of our lobe zone. Indeed, the large deposition zones in the southeast corner of the study area are visibly truncated on the elevation change maps (Fig. 8), as are ones in other sections of the lobe. This leads us to conclude that the effects of the changes in the blowout are more far-reaching than one might expect and this points to the necessity of viewing the system much more broadly in order to establish how the changes in one feature cascade into changes in numerous other features across a broad landscape.

7. Conclusion

This study provides insight into three important components of blowout evolution: 1. blowouts can evolve suddenly and dramatically as a result of capturing adjacent blowouts; 2. the topography of the blowout controls the way in which the feature evolves and the direction of sediment transport out of the blowout; and 3. the capture of another blowout facilitates the contribution of sediment to the landscape far beyond the area identified as the depositional lobe. The majority of geomorphic change is associated with high magnitude/long duration storm events that occur mainly from fall to spring, and particularly those events with wind directions that are aligned with the blowout axis. These times also correspond with the lowest surface vegetation cover as the *Ammophila* dies back or declines in winter. Our data also provide evidence that flow normal to the blowout axis can result in changes to the morphology of the blowout because of the frequency and magnitude of southwest and northeast wind events that occur at this coastal location. Some morphologic zones (rim, sidewall) within the blowout may owe their particular characteristics to secondary flow patterns.

The sudden expansion of the blowout occurs as a result of a form of geomorphic piracy in which two erosional depressions in a dune surface are merged when the larger one captures the smaller one. Like a stream drainage system capture, the new combined blowout form alters flow and sediment transport patterns that then have repercussions across the broader landscape. While our sample size in the current study is limited, our field investigations along with both air reconnaissance and historic aerial photography (see e.g. Abhar et al., 2015), suggest that small rim blowouts are ubiquitous at Provincelands Dunes. The significant impact on the expansion and topographic change occurring at our study site provides a new model in which rapid blowout evolution can occur by the capture of these small saucers, which very rapidly develop into larger bowl blowouts. Our finding shows a clear need to study these features further and improve our understanding of their roles in the continual evolution of dune blowouts, especially given their abundance in coastal dune systems around the world.

8. Acknowledgements

This work was supported by a National Science Foundation grant (# 1024125) to P. Hesp, I. Walker and P. Gares, which facilitated this study. We are thankful to the Cape Cod National Seashore, particularly Dr. Megan Tyrrell and other staff at the Atlantic Research and Learning Center for facilitating access to study sites and encouraging our work. P. Hesp acknowledges

the support of Louisiana State University and Flinders University. The East Carolina Division of Research and Graduate Studies has provided several grants to T. Wasklewicz to facilitate purchase and maintenance of the laser scanning equipment used in this project. The Terrain Analysis Lab at East Carolina University has also provided funds, equipment, software, office space, and data storage to this project. Finally, we thank the numerous students who provided field assistance: K. Reavis, M. Roman-Rivera, M. Haynes, K. Adams, D. Kirk, C. Chapman, K. Abhar.

9. References

Abhar, K.C., Walker, I.J. Hesp, P.A., Gares, P.A., 2015. Spatial-temporal evolution of aeolian blowout dunes at Cape Cod. Geomorphology 236, 148-162. DOI: 10.1016/j.geomorph.2015.02.015

Anderson, J. L. and Walker, I.J., 2006. Airflow and sand transport variations within a backshore-parabolic dune plain complex, NE Graham Island, British Columbia, Canada. Geomorphology 77, 17-34. DOI: 10.1016/j.geomorph.2005.12.008

Andrews, B.D., Gares, P.A., Colby, J.D., 2002. Techniques for GIS modeling of coastal dunes. Geomorphology 48(1-3), 289-308. DOI: 10.1016/S0169-555X(02)00186-1

Bagnold, R.A., 1941. The Physics of Blown Sand and Desert Dunes. Chapman & Hall, London.

Bitelli, G., Dubbini, M., Zanutta, A., 2004. Terrestrial laser scanning and digital photogrammetry techniques to monitor landslide bodies. Int. Arch. Soc. Photogramme. Arch. Rem. S. and Spat. Inf. Sci., 35-B5, 246-251.

Brasington, J., Vericat, D., and Rychkov, I., 2012. Modeling river bed morphology, roughness, and surface sedimentology using high resolution terrestrial laser scanning. Water Resour. Res. 48(11) DOI, 10.1029/2012WR012223

Bressolier, C., and Thomas, Y-F., 1977. Studies on wind and plant interactions on French Atlantic Coastal dune. J. Sedimentary Petrol. 47(1), 331-338. DOI: 10.1306/212F7162-2B24-11D7-8648000102C1865D

Brown, D.G. and Arbogast, A.F., 1999. Digital photogrammetric change analysis as applied to active coastal dunes in Michigan. Photogramm. Eng. Rem. S. 65(4), 467-474. DOI: 0099-1112/99/650446

Bullard, J.E., 1997. A note on the use of the “Fryberger Method” for evaluating potential sand transport by wind. J. Sediment Res. 67 (3), 499-501. DOI: 10.1306/D42685A9-2B26-11D7-8648000102C1865D

Byrne, M-L., 1997. Seasonal sand transport through a trough blowout at Pinery Provincial Park, Ontario. Can. J. Earth Sci. 34, 1460-1466. DOI: 10.1139/e17-118

Carter, R.W.G., Hesp, P.A. and Nordstrom, K.F., 1990. Erosional landforms in coastal dunes. In: Nordstrom, K.F., Psuty, N.P. and Carter, R.W.G. (Eds.), Coastal Dunes, Form and Process. Wiley, London, pp. 217-249.

Cooper, W.S., 1958. The coastal sand dunes of Oregon and Washington. Geological Society of America Memoir 72, Geol. Soc. Am., Boulder, CO.

Darke, I. and McKenna Neuman, C., 2008. Field study of beach water content as a guide to wind erosion potential. J. Coastal Res. 24(5), 1200-1208. DOI: 10.2112/00-000.1

Davidson-Arnott , R.G.D. and Law, M.N., 1990. Seasonal patterns and controls on sediment supply to coastal foredunes, Long Point, Lake Erie. Coastal Dunes, Processes and Geomorphology, New York, Wiley, 177-200.

Davidson-Arnott, R.G.D., Yang, Y., Ollerhead, J., Hesp, P.A. and Walker, I.J., 2007. The effects of surface moisture on aeolian sediment transport threshold and mass flux on a beach. Earth Surf. Proc. Land. 33, 55-74. DOI: 10.1002/esp.1527

Delgado-Fernandez, I., and Davidson-Arnott, R.G.D., 2011. Meso-scale aeolian sediment input to coastal dunes, The nature of aeolian transport events. Geomorphology, 126, 217-232. DOI: 10.1016/j.geomorph.2010.11.005

Dewez, T.J., Rohmer, J., Regard, V. and Cnudde, C., 2013. Probabilistic coastal cliff collapse hazard from repeated terrestrial laser surveys, case study from Mesnil Val (Normandy, northern France). J. Coastal Res. SP65(1), pp.702-707. DOI: 10.2112/SI65-119.1

Dong, Z., Gao, S. and Fryrear, D.W., 2001. Drag coefficients, roughness length and zero-plane displacement height as disturbed by artificial standing vegetation. J. Arid Environ. 49(3), 485-505. DOI: 10.1006/jare.2001.0807

Feagin, R.A., Williams, A.M., Popescu, S., Stukey, J. and Washington-Allen, R.A., 2014. The use of terrestrial laser scanning (TLS) in dune ecosystems, The lessons learned. J. Coastal Res. 30(1), pp.111-119. DOI: 10.2112/JCOASTRES-D-11-00223.1

Folk, R.L., 1966. A review of grain size parameters. Sedimentology 6(2), 73-93. DOI: 10.1111/j.1365-3091.1966.tb01572.x

Forman, S.L., Sagintayev, Z., Sultan, M., Smith, S., Becker, R., Kendall, M. and Marin, L., 2008. The twentieth-century migration of parabolic dunes and wetland formation at Cape Cod National Sea Shore, Massachusetts, USA, landscape response to a legacy of environmental disturbance. Holocene 18 (5), 765-774. DOI: 10.1177/0959683608091796

Fraser, G.S., Bennett, S. W., Olyphant, G. A., Bauch, N.J., Ferguson, V., Gellasch, C.A., Millard, C.L., Mueller, B., O'Malley, P.J., Way, J.N., and Woodfield, M.C., 1998. Windflow Circulation Patterns in a Coastal Dune Blowout, South Coast of Lake Michigan. J. Coastal Res. 14 (2), 451-460.

Fryberger S.G. and Dean, G., 1979. Dune Forms and Wind Regime. In: McKee A Study of Global Sand Seas. U.S. Geological Survey Professional Paper 1052, 137-169.

Gares, P.A. 1992. Topographic changes associated with coastal dune blowouts at island beach state park, New Jersey. Earth Surf. Proc. Land. 17 (6), 589-604. DOI: 10.1002/esp.3290170605

Gares, P.A. and Nordstrom, K.F., 1987. Dynamics of a coastal foredune blowout at Island Beach State Park, NJ. In: Kraus, N.C. (Ed.) Coastal Sediments '87, ASCE, New York, pp. 213-221.

Gares, P. A. and Nordstrom, K.F., 1995; A Cyclic Model of Foredune Blowout Evolution for a Leeward Coast, Island Beach, New Jersey. Annals Assoc. Am. Geog. 85 (1), 1-20. DOI: 10.1111/j.1467-8306.1995.tb01792.xa

Gares, P.A., and Pease, P., 2014. Influence of topography on wind speed over a coastal dune and blowout system, Jockey's Ridge , NC, USA. Earth Surf. Proc. Land. 40 (7), 853-863. DOI: 10.1002/esp.3670

Hansen, E., DeVries-Zimmerman, S., van Dijk, D. and Yurk, B., 2009. Patterns of Wind Flow and Aeolian Deposition on a Parabolic Dune on the Southeastern Shore of Lake Michigan. Geomorphology 105, 147-157. DOI: 10.1016/j.geomorph.2007.12.012

Hesp, P.A., 1999. The beach, backshore and beyond. In: Short, A.D. (Ed.), Handbook of Beach and Shoreface Morphodynamics. John Wiley, Chichester, pp. 145-170.

Hesp, P.A., 2002. Foredunes and blowouts, initiation, geomorphology and dynamics. Geomorphology 48, 245-268. DOI: 10.1016/S0169-555X(02)00184-8

Hesp, P.A., 2011. Dune coasts. In: Wolanski, E. and McLusky D.S. (Eds.), Treatise on Estuarine and Coastal Science, Vol. 3. Academic Press, Waltham, pp. 193-221.

Hesp, P.A. and Hyde, R., 1996. Flow dynamics and geomorphology of a trough blowout. Sedimentology 43(3), 505-525. DOI: 10.1046/j.1365-3091.1996.d01-22.x

Hesp, P.A. and Pringle, A., 2001. Wind flow and topographic steering within a trough blowout. J. Coastal Res. SI 34 (ICS 2000), 597-601. DOI:

Hesp, P. and Walker, I.J., 2012. Three-dimensional aeolian dynamics within a bowl blowout during offshore winds, Greenwich Dunes, Prince Edwards Island, Canada. Aeolian Res. 3, 389-399. DOI: 10.1016/j.aeolia.2011.09.002

Hesp, P. and Walker, I.J., 2013. Coastal Dunes. In: Shroder, D.J, Lancaster, N., Sherman, D.J. and Bass, A.C.W. (Eds), Treatise on Geomorphology, vol. 11 – Aeolian Geomorphology. Academic Press, San Diego, pp. 328-355.

Hodge, R., Brasington, J., and Richards, K., 2009. In Situ characterization of grain-scale fluvial morphology using Terrestrial Laser Scanning. Earth Surf. Proc. Land. 34(7), 954-968. DOI: 10.1002/esp.1780

Hug, C, Krzystek, P. and Fuchs, W., 2004. Advanced lidar data processing with LasTools. *XXth ISPRS Congress*.

Hugenholtz, C.H. and Wolfe, S.A., 2006. Morphodynamics and climate controls of two aeolian blowouts on the northern Great Plains, Canada. Earth Surf. Proc. Land. 31 (12), 1540-1557. DOI: 10.1002/esp.1367

Hugenholtz, C.H. and Wolfe, S.A., 2009. Form-flow interactions of an aeolian saucer blowout. Earth Surf. Proc. Land. 34 (7), 919-928. DOI: 10.1002/esp.1776

Jungerius, P. D. and van der Meulen, F., 1989. The Development of Dune Blowouts, As Measured with Erosion Pins and Sequential Air Photos. Catena 16, 369-376. DOI: 10.1016/0341-8162(89)90021-0

Jungerius, P. D., Verheggen, A. J. T., & Wiggers, A. J., 1981. The development of blowouts in 'De Blink', a coastal dune area near Noordwijkerhout, The Netherlands. Earth Surf. Proc. Land. 6(3-4), 375-396. DOI: 10.1002/esp.3290060316

Kayhko, J. 2007. Aeolian Blowout Dynamics in Subarctic Lapland Based on Decadal Levelling Investigations. Geogr. Ann. A 89 (1), 65-81. DOI: 10.1111/j.1468-0459.2007.00308.x

Langston, G. and McKenna-Neuman, C., 2005. An experimental study on the susceptibility of crusted surfaces to wind erosion, a comparison of the strength properties of biotic and salt crusts. Geomorphology 71(1), 40-53. DOI: 10.1016/j.geomorph.2005.05.003

McKenna-Neuman, C., 1993. A review of aeolian transport processes in cold environments. Prog. Phys. Geog. 17(2), 137-155. DOI: 10.1177/030913339301700203

McKenna-Neuman, C., 2004. Effects of temperature and humidity upon the transport of sedimentary particles by wind. Sedimentology 51(1), 1-17.

McKenna-Neuman, C., and Sanderson, S., 2008. Humidity controls on particle emission in aeolian systems. J. Geophys. Res.-Earth, 113 (F02S14). DOI: 10.1029/2007JF000780

McKenna-Neuman, C., Maxwell, C.D. and Boulton, J.W., 1996. Wind transport of sand surfaces crusted with photoautotrophic microorganisms. Catena, 27(3), 229-247. DOI: 10.1016/0341-8162(96)00023-9

Milan, D.J., Heritage, G.L., Hetherington, D., 2007. Application of a 3D laser scanner in the assessment of erosion and deposition volumes and channel change in a proglacial river. Earth Surf. Proc. Land. 32(11), 1657-1674. DOOI: 10.1002/esp.1592

Nield,J.M., and Wiggs, G.F.S., 2011. The application of terrestrial laser scanning to aeolian saltation cloud measurement and its response to changing surface moisture. Earth Surf. Proc. Land. 36 (2), 273-278. DOI: 10.1002/esp.2102

Nield, J.M., Wiggs, G.F.S., and Squirrell, R.S., 2011. Aeolian sand strip mobility and protodune development on a drying beach, examining surface moisture and surface roughness patterns measured by terrestrial laser scanning. Earth Surf. Proc. Land. 36 (4), 513-522. DOI: 10.1002/esp.2071

Oke, T.R., 1978. Boundary Layer Climates. Methuen and Co., London, 372.pp.

Ollerhead, J., Davidson-Arnott, R., Walker, I.J., and Mathew, S., 2013. Annual to decadal morphodynamics of the foredune system at Greenwich Dunes, Prince Edward Island, Canada. Earth Surf. Proc. Land. 38, 284-298. DOI: 10.1002/esp.3327

Olsen, M.J., Johnstone, E., Driscoll, N., Ashford, S.A. and Kuester, F., 2009. Terrestrial laser scanning of extended cliff sections in dynamic environments, Parameter analysis. J. Surv. Eng. 135(4), pp.161-169. DOI: 10.1061/(ASCE)0733-9453(2009)135:4(161)

Olson, J.S., 1958. Lake Michigan dune development, Wind velocity profiles. J. Geol. 66, 254-263. DOI: 10.1086/626503

Parsons, D.R., Walker, I.J., and Wiggs, G.F.S., 2004. Numerical modeling of flow structures over idealized transverse aeolian dunes of varying geometry. Geomorphology, 59, 149-164. DOI: 10.1016/j.geomorph.2003.09.012

Pearce, K.I. and Walker, I.J., 2005. Frequency and magnitude biases in the 'Fryberger' model, with implications for characterizing geomorphically effective winds. Geomorphology, 68 (1-2), 39-55. DOI: 10.1016/j.geomorph.2004.09.030

Pease, P. and Gares, P.A., 2013. The influence of topography and approach angles on local deflections of airflow within a coastal blowout. Earth Surf. Proc. Land. 38 (10), 1160-1169. DOI: 10.1002/esp.3407

Pietro, L.S., O'Neal, M.A. and Puleo, J.A., 2008. Developing terrestrial-LIDAR-based digital elevation models for monitoring beach nourishment performance. J. Coastal Res. 24(6), pp.1555-1564. DOI: 10.2112/07-0904.1

Pluis J. L. A. 1992. Relationships between deflation and near surface wind velocity in a coastal dune blowout. Earth Surf. Proc. Land. 17, 663-673. DOI: 10.1002/esp.3290170703

Resop, J.P. and Hession, W.C., 2010. Terrestrial laser scanning for monitoring streambank retreat, Comparison with traditional surveying techniques. J. Hydraul. Eng.-ASCE, 136(10), pp.794-798. DOI: 10.1061/(ASCE)HY.1943-7900.0000233#sthash.FtmyO6hZ.dpuf

Schatz, V. and Herrmann, H.J., 2006. Flow separation in the lee side of transverse dunes, A numerical investigation. Geomorphology, 81, 207-216. DOI: 10.1016/j.geomorph.2006.04.009

Scheinert, C., Wasklewicz, T. and Staley, D., 2012. Alluvial fan dynamics – Revisiting the field. Geography Compass, 6(12), 752-775. DOI: 10.1111/gec3.12004

Smyth, T.A.G., Jackson, D.W.T., and Cooper, J.A.G., 2012. High resolution measured and modeled three-dimensional airflow over a coastal bowl blowout. Geomorphology, 177-178,62-73. DOI: 10.1016/j.geomorph.2012.07.014

Smyth, T.A.G., Jackson, D.W.T., and Cooper, J.A.G., 2013. Three-dimensional airflow patterns within a trough bowl blowout during fresh breeze to hurricane force winds. Aeolian Res. 9, 111-123. DOI: 10.1016/j.aeolia.2013.03.002

Smyth, T.A.G., Jackson, D.W.T., and Cooper, J.A.G., 2014. Airflow and aeolian sediment transport patterns within a coastal trough blowout during lateral wind conditions. Earth Surf. Proc. Land. 39(14), 1847-1854. DOI: 10.1002/esp.3572

Staley, D., Wasklewicz, T., Coe, J., Kean, J., McCoy, S., and Tucker, G.E., 2011. Observations of debris flows at Chalk Cliffs, Colorado, USA, Part 2, changes in surface morphometry from terrestrial laser scanning in the summer of 2009. Proc. 5th Int. Conf. Debris Flow Haz. Mit. Mech. Pred. Assess., Ital. J. Eng. Geology and Env., 759-768. DOI: 10.4408/IJEGE.2011-03.B-083

Staley, D., Wasklewicz, T., and Kean, J. 2014. Characterizing the primary material sources and dominant erosional processes for post-fire debris-flow initiation in a headwater basin using multi-temporal terrestrial laser scanning data. Geomorphology, 214, 324-338. DOI: 10.1016/j.geomorph.2014.02.015

Sweet, M.L. and Kocurek, G., 1990. An empirical model of aeolian dune lee-face airflow. Sedimentology, 37(6), 1023-1038. DOI: 10.1111/j.1365-3091.1990.tb01843.x

Walker, I.J., 1999. Secondary airflow and sediment transport in the lee of reversing dunes. Earth Surf. Proc. Land. 24, 437-448. DOI: 10.1002/(SICI)1096-9837(199905)24:5<437::AID-ESP999>3.0.CO;2-Z

Walker, I.J. and Nickling, W.G., 2002. Dynamics of secondary airflow and sediment transport over and in the lee of transverse dunes. Prog. Phys. Geog. 26(1), 45-75. DOI: 10.1191/0309133302pp325ra

Walker, I.J., and Nickling, W.G., 2003. Simulation and measurement of surface shear stress over isolated and closely spaced transverse dunes in a wind tunnel. Earth Surf. Proc. Land. 1111-1124. DOI: 10.1002/esp.520

Walker, I.J. and D.H. Shugar, 2013. Secondary flow deflection in the lee of transverse dunes with implications for dune morphodynamics and migration. Earth Surf. Proc. Land. 38, 1642-1654. DOI: 10.1002/esp.3398

Wasklewicz, T.A. and Hattanji, T. 2009. High-Resolution Analysis of Debris Flow–Induced Channel Changes in a Headwater Stream, Ashio Mountains, Japan. Prof. Geogr. 61(2), 231-249. DOI: 10.1191/0309133302pp325ra

Wasklewicz, T. and Scheinert, C., 2016. Development and maintenance of a telescoping debris flow fan in response to human induced fan surface channelization, Chalk Creek Valley Natural Debris Flow Laboratory, Colorado, USA. Geomorphology, 252, 51-65. DOI: 10.1016/j.geomorph.2015.06.033

Wasklewicz, T.A.. Zhu, Z., and Gares, in print. Simulating and Quantifying Legacy Topographic Data Uncertainty, An Initial Step to Advancing Topographic Change Analyses. Prog. Earth Planet Sci.

Wester, T.B., Wasklewicz, T., and Staley, D.S., 2014. Functional and structural connectivity within a recently burned drainage basin. Geomorphology, 206, 362-373. DOI: 10.1016/j.geomorph.2013.10.011

Yurk, B., Hansen, E.C., DeVries-Zimmerman, S., Kilibarda, Z., van Dijk, D., Bodenbender, B., Krehel, A., Pennings T., 2014, The role of extratropical cyclones in shaping dunes along southern and southeastern Lake Michigan. In: Fisher, T.G., and Hansen, E.C., (Eds.), Coastline and Dune Evolution along the Great Lakes. Geological Society of America Special Paper 508, p. 167–194, doi,10.1130/2014.2508(10).

List of Figures

color of the circle. Grey lines on the roses identify the sediment drift potential (DP) for different wind directions (as a percentage of total predicted drift). Black line with arrow shows the resultant sediment transport direction (RDD). Pie wedges represent total erosion (sediment removal) along each transect (as a percentage of the total observed erosion). RDD (solid) and resultant erosion vector (dashed) for each year are represented on blowout DEM.

Figure 10: A - Likely airflow patterns under northeast wind approach to the study blowout; B - Likely airflow patterns under southwest wind approach to the study blowout.

Figure 1

Figure 2

Figure 3

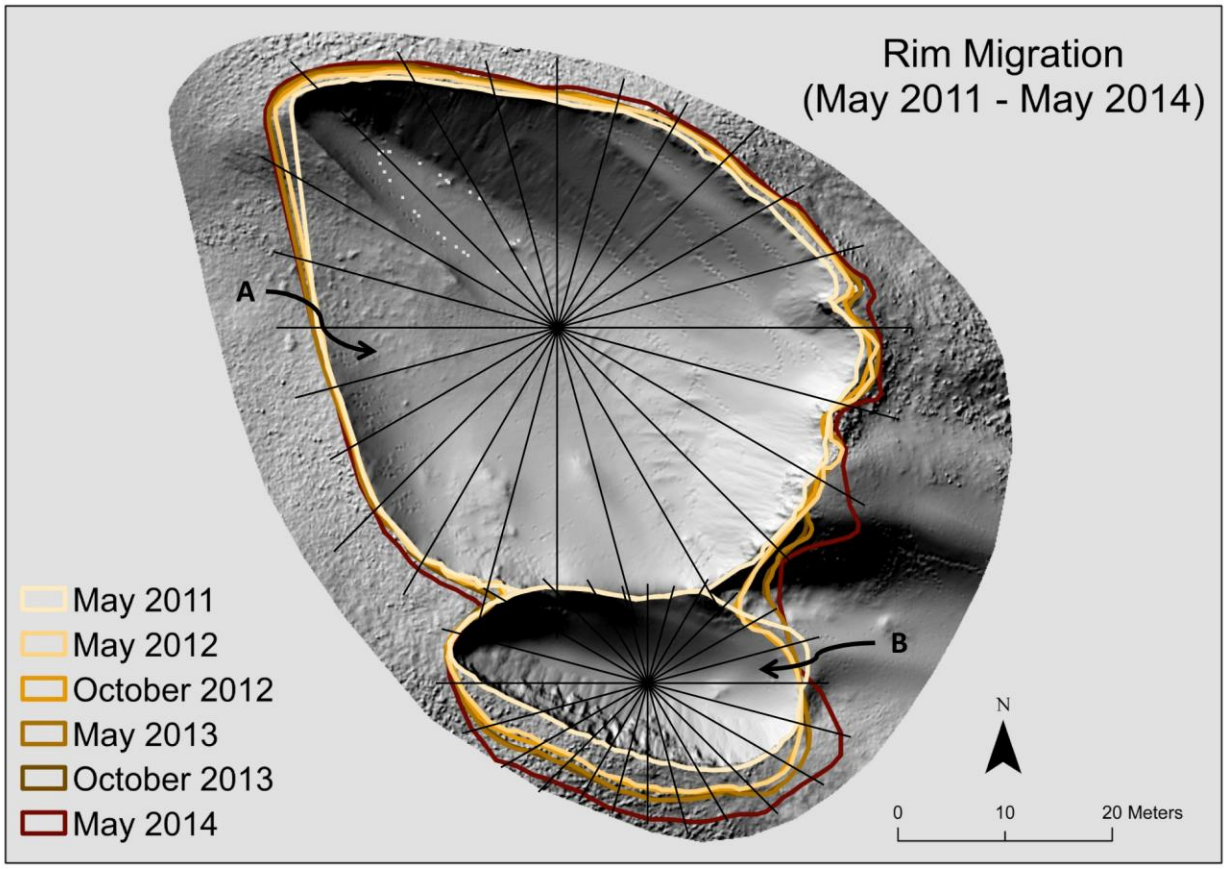

Figure 4

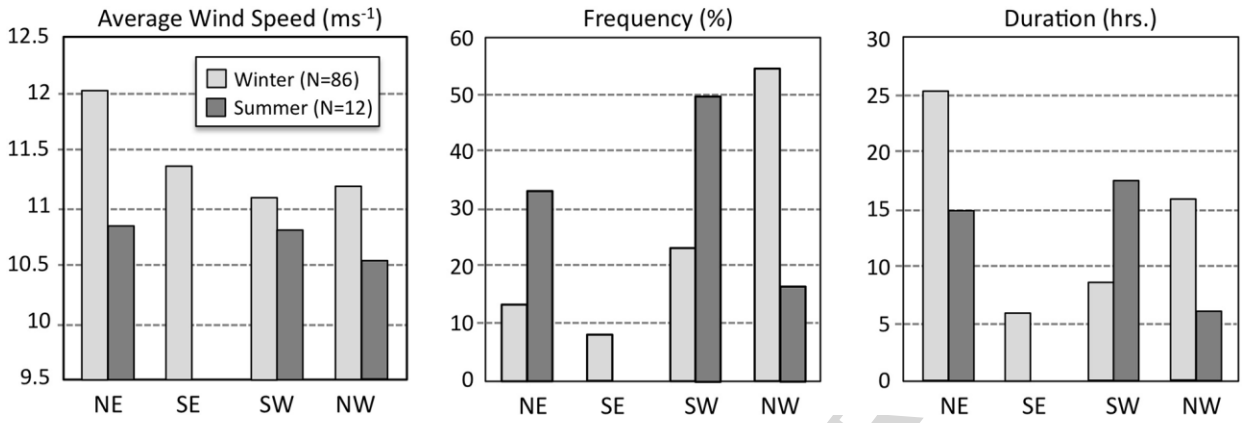

Figure 5

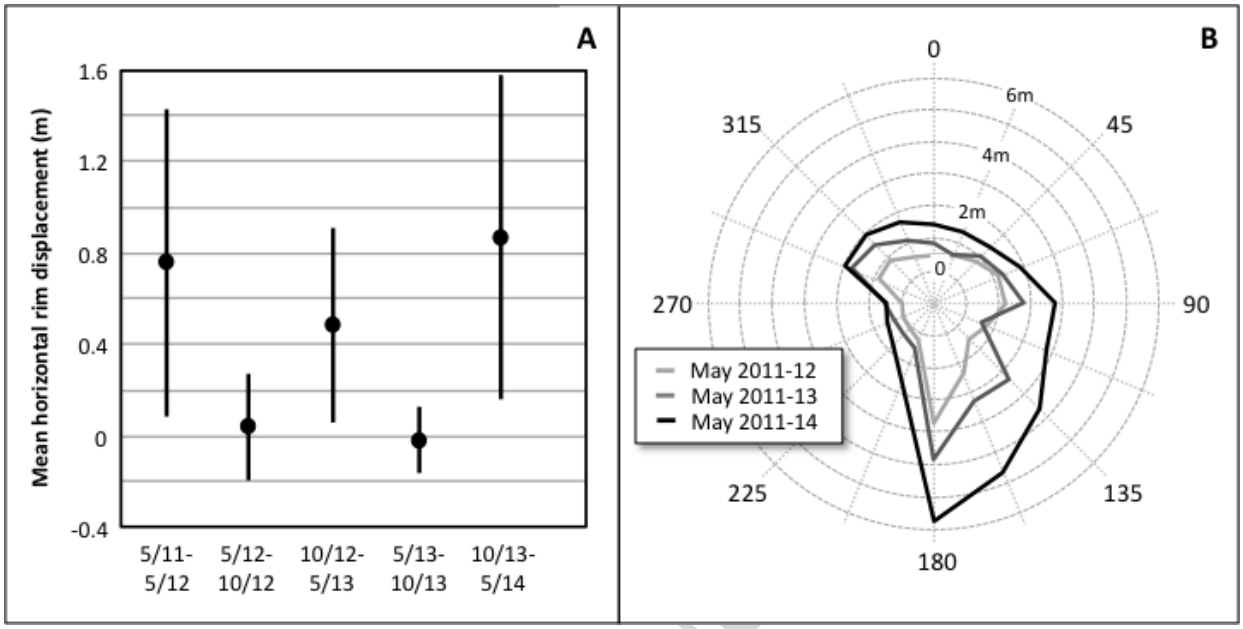

Figure 6

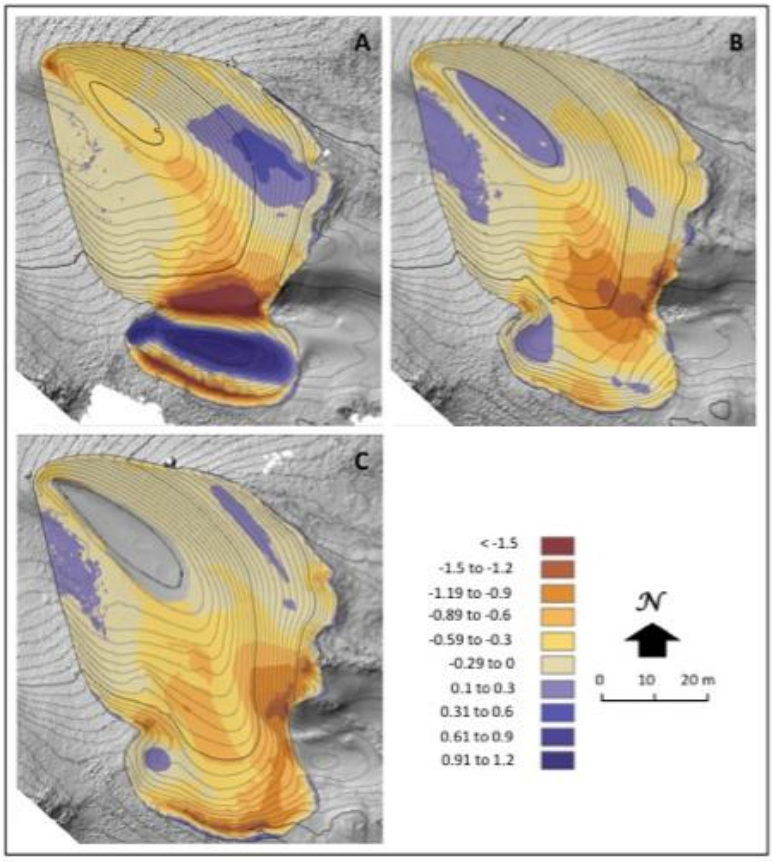

Figure 7

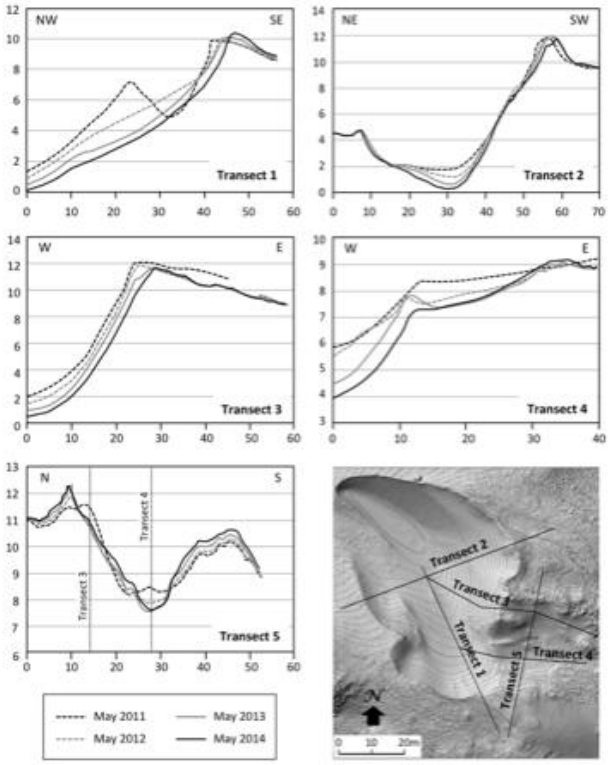

Figure 8

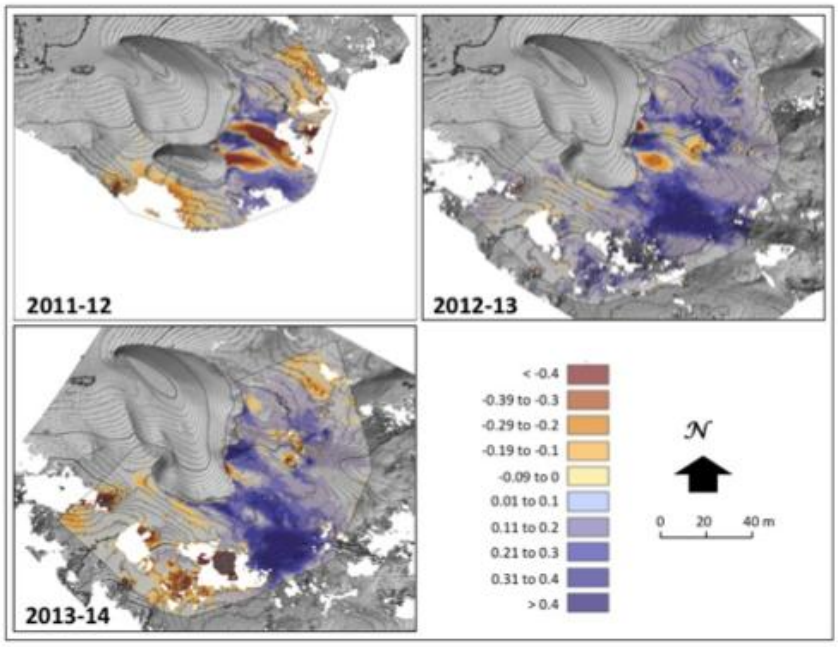

Figure 9

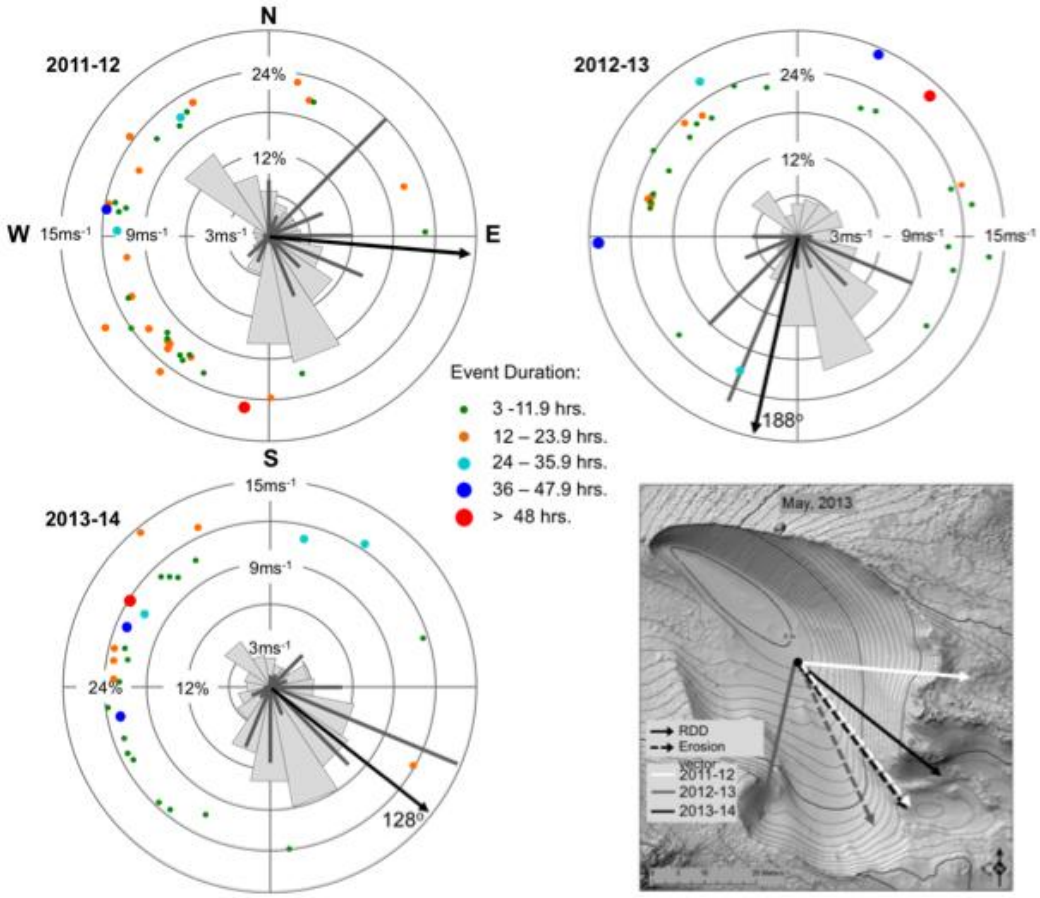

Figure 10